Why a steady void size distribution in irradiated UO_2? A modeling approach.

S. Maillard, G. Martin, C. Sabathier-Devals

Why a steady void size distribution in irradiated UO_2? A modeling approach.

S. Maillard[a,*], G. Martin[a,b], C. Sabathier[a]

[a] *CEA, DEN, SESC, LLCC, F-13108 St Paul lez Durance, France*
[b] *CEA, DEN, SPRC, LEC, F-13108 St Paul lez Durance, France*

Abstract

In UO_2 pellets irradiated in reactor, Xe nano-bubbles nucleate, grow, coarsen and finally reach a quasi steady state size distribution (transmission electron microscope observations typically report a concentration around $10^{-4}\,nm^{-3}$ and a radius around 0.5 nm). This phenomenon is often considered as a consequence of radiation enhanced diffusion, precipitation of gas atoms and ballistic mixing. However, 4 MeV Au ion irradiation of UO_2 thin foils at room temperature yields a nano-void population whose size distribution reaches a similar steady state, although quasi no foreign atoms are implanted nor significant cation vacancy diffusion expected at such temperature and ion energy. Atomistic simulations performed at low temperature support the assumption of heterogeneous nucleation: 25 keV sub-cascades produce defect aggregates that grow through sub-cascade overlapping. In this work a semi-empirical model is proposed to extend these results to the simulation of the size distribution evolution of a representative defect aggregates population in a fraction of a material grain under a cascade overlap regime. To account for the damage accumulation when cascades overlap, this model is based on simple rules inferred from the atomistic simulation results. It satisfactorily reproduces the TEM observations of nano-voids size and concentration, which paves the way for the introduction of a more realistic damage term in rate theory models.

Keywords: Fission gas bubbles, UO_2, Irradiation effects, Object Kinetic Monte Carlo, Irradiation cascade.

*Corresponding author
Email address: serge.maillard@cea.fr (S. Maillard)

1. Introduction

Fission gases produced in irradiated nuclear fuel materials such as UO_2 may have detrimental effects on the fuel rod integrity due to excessive loading of the cladding, either when gas release increases the rod pressure, or when high temperature events enhance the pellet swelling. For this reason, extensive studies of fission gas behavior in UO_2 under irradiation were developed over decades. They progressively achieved a clearer description of the phenomena, but a global understanding of the controlling mechanisms is still in progress. This paper is focused on the buildup of the cavity or bubble quasi steady state size distribution arising from the in pile irradiation of the external and colder zone of a fuel a pellet, but also in other situations as will be seen below. The issue will be addressed through the modeling of the cavity growth process under ion irradiation as observed in a transmission electron microscope (TEM). This represents a first step in solving the more complex question of in-pile generated bubbles.

In fact, as reported for example in the review of [4], TEM observations of in-pile irradiated UO_2 [26, 2] show bubbles appearing in bulk UO_2 at fission densities around $10^{-2}\,\mathrm{nm}^{-3}$, rapidly coarsening and growing until their size distribution finally reaches a quasi steady state. The average radius $\bar{R}$ and concentration $\bar{C}$ lay in the ranges of $\bar{R} \sim 0.5\,\mathrm{nm}$, $\bar{C} \sim 10^{-4}\,\mathrm{nm}^{-3}$ respectively. Further studies [7] exploring a wider range of temperature and burn-up show that the cavity size distribution evolves slowly with fission density or temperature while staying in the same range (for this reason we will generally omit the word "quasi" in front of "steady state"). To allow deeper investigation of the material, mock-up experiments were undertaken, such as in-situ thin foils irradiation with accelerated ions. For example in [15], UO_2 foils implanted with 390 keV Xe ions at 600 °C also show a steady state cavity distribution moreover very similar to that of in-pile irradiated samples. Additionally this low energy ion irradiation experiment does not support the often claimed hypothesis of bubble "heterogeneous nucleation" in the wake of fission fragments, which reactivates the question of the bubble nucleation mechanism. Other investigations gave important information on this issue:

- Similar experiments with non gaseous ions (irradiation with 300 keV Cs ions at RT [21]) yielded the same cavity evolution . This suggests that the previously observed cavities may not contain gas and raises questions on the reality of the "homogeneous nucleation" alternative mechanism supposing bubbles nucleate when two gas atoms collide during the diffusion process. XANES analysis of samples similarly implanted with Xe ions proves the cavities are practically devoid of gas [1]. This conclusion was confirmed by irradiation with 4 MeV Au ions of UO_2 foils too thin to allow significant Au implantation: the same cavity pattern has been observed. This clearly indicates that the origin of the cavity nucleation is to be first sought in the damage process and not in the implanted foreign atoms. Moreover, these results keep raising questions concerning the cavity growth mechanism: growth requires cation vacancies gathering but

in these conditions, no diffusion is expected (see discussion), so that the gathering mechanism is questionable.

– Various classical molecular dynamics (CMD) simulations of cascades in UO_2 shed some light on both the issues of cavity nucleation and growth [11, 10, 12, 27, 28]. A global picture of the damage process can be drawn [10, 4, 23]. An ion beam produces a displacement cascade that finally splits into independent "sub-cascades" starting at an energy of $\sim 25\,\mathrm{keV}$, each producing a disordered and very hot zone of volume around a few hundreds of nm^3. This zone finally anneals out in a damaged crystalline zone comprising approximately one hundred Frenkel pairs (O and U isolated or clustered vacancies and interstitial atoms); larger clusters such as one cavity of 10 to 20 vacancies and one or two loops of 10-20 interstitial atoms occupy the center and the periphery respectively of the previously disordered zone. In addition, the central cavity volume grows in proportion to the number of sub-cascade overlaps in the simulation box ([10] Fig. 7).

The global analysis (e.g. [4]) of these results suggests that the irradiation effect results from successive independent sub-cascades in which cavities and loops directly nucleate without requiring foreign atoms and that these defect clusters can grow through sub-cascade overlaps in the absence of cation migration. Nevertheless, the last point concerning the cavity radius evolution during sub-cascade overlapping is not consistent with the experimental results: in the CMD simulations, the cavity average radius does not level off after 36 overlaps and exceeds the experimental saturation value of $\sim 0.5\,\mathrm{nm}$. This discrepancy may come from the fact that the simulation box is too small for overlapping simulation: the same material zone is systematically overlapped, while in reality, a sub-cascade can connect and anneal zones of the material with different damage characteristics (for ex. a vacancy-rich zone and an interstitial atom rich zone) which finally should impact the growth rate of the defect clusters. An appropriate way to study this growth rate would be intensive CMD simulations in a box large enough to house several independent disordered zones. As the computing cost for such a simulation is high and as an analytical formulation of the damage is eventually sought for fuel performance assessment codes, an alternative modeling strategy is proposed. The rest of this paper will then present and assess a semi-empirical model of the sub-cascade overlapping.

2. The model

The basic idea of this sub-cascade overlap model is that when a new sub-cascade impacts an already damaged zone, the existing damage is first annealed (because of the high temperature generated by the sub-cascade), and the damage surviving to the annealing process is then added to that created by the new sub-cascade. In the model, the space is discretized in cubic voxels, each schematically representing a "site" or UO_2 pattern (of volume $0.043\,nm^3$), no detail is considered below this pattern so that U and O atoms are not considered separately: all defects are supposed stoichiometric. This might be a crude approximation for the smaller sizes, as for example non-stoichiometric (thus charged) defect aggregates appear as a result of CMD simulations (e.g [10]) although the interatomic potential does not allow the charge transfer liable to reduce the energy cost of such non-stoichiometric clusters. Nevertheless, at room temperature and above, the migration of charge and oxygen vacancies or interstitial atoms should be fast enough to enable rapid relaxation of local departure from the exact stoichiometry. At last, the proposed model is aimed at giving a general picture of the irradiation damage accumulation; considering the very high sub-cascade energy compared to the ionization and binding energies of defects, the main characteristics of the primary damage (total number of O or U defects, volume of aggregates) should not be very much affected by the possibility or not of ionization and departure from stoichiometry.

In this respect the damage is composed of sets of Schottky ($V_U(V_O)_2$) and anti-Schottky ($U_i(O_i)_2$) defects, respectively stated as "vacancies" or "interstitials atoms" and accordingly coded by a number $\xi_i = \pm 1$ at the defect position in space (labeled by i); $\xi_i = 0$ for undamaged voxels. Sub-cascades are successively generated at random positions, for each occurrence the resulting damage is evaluated. Any sub-cascade generates a cubic disordered zone of volume V^s (n^s voxels) in which the ξ_i are updated according to the CMD results for sub-cascade simulations ([10] Fig. 6) in a simplified way. The primary damage is the same for all sub-cascades: one cavity at the center, one loop at the periphery and some tens of isolated "vacancies" (Schottky) and "interstitial atoms" (anti-Schottky). In the case of an initially undamaged piece of material, a total number of n^p pairs of Schottky - anti-Schottky defects are generated, among which $n^p - n^c$ vacancies and $n^p - n^c$ interstitial atoms are isolated and randomly dispersed in the volume V^s (the vacancy preferentially occupying the center of the disordered zone while the interstitial atoms lying more in the periphery). The remaining n^c vacancies are clustered: a cubic cavity of volume V^c (n^c vacancies with $\xi_i = -1$) is created at the center. Symmetrically the n^c interstitial atoms cluster in a square shaped loop inserted near one of the faces of the zone (n^c interstitials for which $\xi_i = 1$)[1]. Figure 2 shows the first occurrences of the simulated damage process (isolated defects are omitted) and

[1] The sizes of the cavity and loop could be slightly different. For simplicity they were supposed equal (to n^c) in this version of the model.

the model parameters are summarized in Table 1. When the impact zone of the sub-cascade is already damaged, the annealing step is first simulated supposing that a defect annihilates if there is a defect of opposite sign in the disordered zone. The surviving net damage δn in the algebraic sum of the defects initially present in the zone: $\delta n = \sum_{i \epsilon V^s} \xi_i$. This yields a loop (of size δn) if $\delta n > 0$, a cavity of size $-\delta n$ in the opposite case. Secondly, this net damage is added to the new damage described above, finally yielding a cavity of $n^c + |\delta n|$ vacancies and a loop of n^c interstitials if $\delta n < 0$ or a cavity of n^c vacancies and a loop of $n^c + |\delta n|$ interstitials if $\delta n > 0$. The $2\,(n^p - n^c)$ isolated defects are added at random positions in the volume V^s (the vacancies being closer to the center of the disordered zone). Finally, as interstitial atoms are supposed to be very mobile at room temperature [25, 24], a thermal annealing step is processed between two successive sub-cascades following an object kinetic Monte Carlo (OKMC) procedure which interstitial atoms diffuse and can be irreversibly trapped by other defects. Considering Δt_b as the average time period between two successive sub-cascades, the program creates for each sub-cascade (at date t) a list of all the random diffusion events [8] (here anti-Schottky defects diffusion) occuring in the time interval $[t, t + \Delta t_b]$. These events are successively activated (each corresponding anti-Schottky is moved to its calculated final position) before a new random sub-cascade is created at $t + \Delta t_b$.

3. An application of the model

The model has been applied to the irradiation of a UO_2 foil with 4 MeV Au ions at room temperature [20].

3.1. Model parameters

Most of the model parameters were derived from studies implying various simulation techiques.

The sub-cascade energy was set to $E_s = 25\,\text{keV}$ according to the analysis in [4, 23] based both on CMD and BCA calculation. This is somehow simplified as it does not simultaneously consider the U and O atoms nor variability of this energy from a cascade event to another; a deeper analysis should lead to a refined value of this energy, which in turn would slightly impact the number of point defects generated by an average sub-cascade.

The primary damage characteristics for a 25 keV sub-cascade were extrapolated on the basis of CMD simulations. They comprise the total number of pairs of defects ($n^p = 50$), the size of the larger cavity or loop ($n^c = 3$ Schottky volumes) [11], and the size of the disordered zone ($n^s = 3375$ Schottky volumes at 300 K) [13].

For the OKMC model, the anti-Schottky migration energy was estimated to $E_m = 0.7\,\text{eV}$ and the diffusion pre-factor ($D_0 = 1.22\,\text{nm}^2/\text{ps}$) is based on a frequency close to the Debye frequency ([24, 9] which give orders of magnitude similar to [25]).

3.2. Experiment characteristics

The larger part of the ballistic energy effectively deposited in the foil and responsible for the sub-cascades is that lost by the ion beam and is to the first order proportionnal to the thickness h. But for low values of h a significant part of the displaced atoms eventually leave the material through sputtering and reduce the cascade yield. The effectively deposited ballistic energy E_b as a function of the thickness (Figure 1 and Table 1) has been estimated on the basis of ten SRIM [31] simulations of a 4 MeV Au beam in foils of thickness ranging form 10 to 100 nm. Technically this energy has been computed as the difference between the ballistic loss of the beam and the total energy carried by both the "sputtered" and "transmitted recoil ions" as described in the corresponding SRIM output files.

The thickness h of the foil is thought to be in the range $10 - 50$ nm on the basis of EELS measurements of similar samples; the simulation results will help fitting this parameter as will be seen below.

For irradiation with ions transferring a ballistic energy E_b to the material, the fluency F in a foil of thickness h is related to the number i of sub-cascades of energy E_s in the simulation cell of volume V^t through the differential equation $dF\frac{V^t}{h}\frac{E_b}{E_s} = di$.

In the same idea, the time interval between two sucessive sub-cascades in the simulation cell is $\Delta t_b = {}^1\!/\!\left(\frac{\dot{F}}{h}\frac{E_b}{E_s}V^t\right)$.

3.3. Results

Several analysis of the model simulation were done, each with a value of the thickness h ranging from 10 to 100 nm. The value $h = 20$ nm was selected as allowing the best fit for the cavity concentration and size distribution on the basis of the different versions of Figures 4 and 6 (only the version with $h = 20$ nm is displayed here). h is the only fitted parameter in the process, all the other ones are determined on the basis of measurements or simulations.

Figure 3 shows the simulated distribution of size (here the number of Schottky or anti-Schottky defects) for cavities and loops at 3000 steps (all the results are actually averages on 10 successive time-steps in order to smooth the time evolution). At smaller sizes, the cavity and loop distributions strongly differ: while wandering by diffusion, the interstitial atoms eventually encounter either a cavity and annihilate (the cavity shrinks) or a loop (which grows). The larger size region of the distribution graph is less concerned because large clusters represent a negligible trapping cross section.

Figure 4 is an analysis of the void size (here radius) distribution for a fluency of $0.76\,\mathrm{nm}^{-2}$. The purple squarish graph represents the experimental data [20], the light blue one is the raw histogram of the simulation results. Each smoothed graph presents the simulated size distribution that should be observed in a TEM image assuming $^{1)}$various values R_{TEM} for the optical resolution for cavities (which is not very well known) and $^{2)}$a 0.025 nm (~ 2 pixels) uncertainty in the

cavity radius (see caption). A resolution of $R_{TEM} \sim 0.35 - 0.40\,\mathrm{nm}$ is consistent with the experimental observations as can be seen in the next two figures.

Figure 5 displays the same comparison on a large range of fluency (between 0.076 and $1.\,\mathrm{nm}^{-2}$). The agreement is best for the larger fluencies ($F > 0.22\,\mathrm{nm}^{-2}$), provided the snapshot for $F = 0.57\,\mathrm{nm}^{-2}$ is considered as an outlier. For smaller fluencies ($F < 0.17\,\mathrm{nm}^{-2}$), the model does not work so well: the total cavity concentration is generally overestimated and the average size is overestimated or underestimated without a clear tendency. This might be explained by the small number of cavities that are created either in the experiment or in the simulation, which produces statistical fluctuations of both simulated and experimental quantities.

Figure 6 displays a realistic evolution of the total cavity concentration for various threshold values R_{TEM}, also confirming the best value of R_{TEM} lies in the range $0.35 - 0.40\,\mathrm{nm}$.

In conclusion, for a foil thickness $h = 20\,\mathrm{nm}$, the model presented here reproduces in a satisfactoy way the experimental data and provides a plausible explanation for the nucleation and growth of nano-cavities under ion beam irradiation in the absence of thermal or irradiation-induced diffusion.

4. Discussion

We will first briefly discuss the possibility for the cavities to grow by diffusion and secondly address the perspectives of applying this kind of model to the modeling of fission gases behaviour.

As stated in the introduction, a brief analysis of the diffusion processes shows that neither of the thermal or irradiation induced diffusion mechanisms of the cation can explain the gathering of the cation vacancies surviving to the cascades during the 400 s of the experiement:

- According to [14, 29], the order of magnitude of the thermal diffusivity would be $D_{thermal} \sim 10^{-39}\,\mathrm{nm}^2/\mathrm{s}$, yielding a diffusion length around $10^{-18}\,\mathrm{nm}$.

- The irradiation induced diffusivity comprises of a ballistic a non-ballistic contribution. According to [12], the ballistic term writes:

$$D_{ballistic} = \frac{1}{2}\frac{\dot{F}}{h} E_b R_0^2 \Omega = 2 \times 10^{-4}\,\mathrm{nm}^2/\mathrm{s}$$

  where $R_0^2 = 6.5\,\mathrm{nm}^2/\mathrm{keV}$ is the ratio between the square displacement and the ballistic energy of a beam (as deduced from Figure 5.b of [12]). The related diffusion length is around 0.3 nm.

- A model for the electronic (thermal spike) contribution linking the electronic energy loss of the ion and the diffusivity is proposed in [3] (eq. (12)

and (18)). The model parameters are taken in Table 5 of [3], except for values specific to this application: the range $\mu = 20\,\text{nm}$ (order of magnitude of the foil thickness) and the electronic energy per ion $E = 54\,\text{keV}$ (electronic energy loss calculated with SRIM for a foil thickness of 20 nm, cf. Fig 1).

The diffusion distances corresponding to the various possible diffusion mechanisms above are thus insufficient to explain the so big observed cavities. The mechanism proposed in this paper appears an appropriate alternative explanation.

Let us now consider the problem of fission gases, which appears to be somehow superimposed to the cavity production issue.

According to our simulation results, the TEM detects only a small part (1.7 %) of the defect clusters, which represents 10 % of the total vacancy volume ("porosity"). This means that if this model was in some way to be applied also to in-pile irradiation at low temperature (immobile cation vacancies), it is quite possible that the TEM observed cavities are devoid of Xe atoms because these atoms are likely to be trapped by the very small and abundant cavities as stated through XANES experiments [1].

The model also suggests ideas to explain similarities, and also differences, of the steady state distribution in many situations as stated in the introduction. In all these situations, the ion beams or fission fragments create similar 25 keV sub-cascades that have the same primary damage impact thus possibly yielding the same steady state distribution. Moreover, if the sub-cascade production is the only phenomenon affecting the micro-structure of the material (e. g. at very low temperature where no migration at all is expected) the evolution of the latter should be a function of the damaged volume fraction only; low temperature experiments would help validate this idea. In the opposite case (e.g. when the material is annealed between sub-cascades), other parameters not directly related to sub-cascades (such as defect diffusivity, or gas solubility) could account for variations in the material's behavior and the micro-structure evolution may be accounted for by various time scales, depending on which defects are mobile at the considered temperature.

In the case of rare gas incorporation (through fission or ion implantation), the model needs to be adapted because gas atoms interact with the defects, moreover (cation) vacancies also diffuse at higher temperature relevant to many in-pile irradiation situations. Although several options are open for modeling sub-cascades interaction with cavities and loops in the vicinity of gas atoms, such a model may provide an interesting alternative to mechanisms often invoked in the literature to explain the steady state bubble distribution during in-pile irradiation.

– For instance, the interpretation of Russel or Veshchunov [19, 30] for the steady state distribution relies on an analysis of the nodal lines in the diagram (bubble gas content) VS (bubble-volume) obtained in the framework

of rate theory equations; the steady state occurs at the intersection of such nodal lines at a stable critical point. In their analysis the presence of gas appears essential to the steady state regime as it allows for two lines intersection, which would not occur in this framework if only self point-defects were considered (corresponding to the bubble volume only). The interpretation of the present article does not require gas atoms in principle and might be relevant also for the cases studied by these authors. Assessing the relevance of the various interpretations in an irradiation simulation would be of high interest.

– Furthermore, the bubble steady state of certain models of fission gas behavior [18, 17] is grounded on a gas re-solution mechanism either "homogeneous" (ballistic) or "heterogeneous" (induced by thermal spikes). None of these mechanisms appear to be well understood yet: for example [1)]the ballistic term as calculated in [16] has been recently reevaluated and shown to be overestimated of a factor as large as 50 [22]; [2)]the heterogeneous term has been evaluated by various CMD approaches whose conclusions do not agree [6, 5]. Taking into account the mechanism described here and the fact that the "bubbles" could be devoid of gas atoms, in addition to a better account of point defects and small clusters for in-pile irradiation situations might also help re-assess the relevance of the various re-solution models .

5. Conclusion

A model for damage accumulation in UO_2 under irradiation is proposed to account for the fact that, during irradiation of a thin foil at room temperature in the ballistic regime, nanometer sized cavities appear and reach a quasi steady state size distribution although no gas is implanted and no cation diffusion is expected. The basic ideas of the model are:

– any displacement cascade is split into equivalent sub-cascades of $\sim 25\,\mathrm{keV}$, each producing a highly disordered region in the material that eventually imperfectly recrystallizes, leaving isolated point defects, a small cavity and a small loop;

– the overlapping of a new sub-cascade on an already damaged zone first anneals the defects included in the zone and secondly accumulates the damage surviving to the annealing with that associated to the new sub-cascade;

– in addition to the sub-cascade driven processes, the material's microstructure evolves under thermal migration of the interstitial atoms; this process is simulated through an Object Kinetic Monte Carlo algorithm.

The simulated evolution of the cavity size distribution compares favorably with the TEM in-situ observations at various fluencies in the case of an irradiation

with 4 MeV Au ions which is encouraging since the only fitted parameter of our model is the foil thickness. In particular, the simulated steady state size distribution is similar to the observations at the same fluency. The cavity nucleation mechanism and growth is consistent with a heterogeneous nucleation mechanism for fission gas bubbles.

The quasi steady state cavity distribution is not very sensitive to the experimental conditions (namely the beam energy and flux, and to a lesser extend the temperature). This could be accounted for by the fact that the displacement cascades split in any situation in 25 keV sub-cascades which are actually responsible for the primary damage in the material. By the way, if the mechanism proposed here is confirmed to be relevant in the case of fission product irradiation (which remains to be done), it could contribute to explaining the quasi steady size distribution during in-pile irradiation in an alternative or complementary way as invoked in various fission gas codes, such as irradiation-induced resolution or stable nodes in the diagram (bubble gas content) VS (bubble volume).

[1] Bès, R., Martin, P., Vathonne, E., Delorme, R., Sabathier, C., Freyss, M., Bertolus, M., Glatzel, P., 2015. Experimental evidence of Xe incorporation in Schottky defects in UO2. Applied Physics Letters 106 (11), –. 2, 8

[2] Cornell, R., Mar. 1971. An electron microscope examination of matrix fission-gas bubbles in irradiated uranium dioxide. JNM 38 (3), 319–328. 2

[3] Ferry, C., Lovera, P., Poinssot, C., Garcia, P., Nov. 2005. Enhanced diffusion under alpha self-irradiation in spent nuclear fuel: Theoretical approaches. Journal of Nuclear Materials 346 (1), 48–55. 7, 8

[4] Garcia, P., Martin, G., Sabathier, C., Carlot, G., Michel, A., Martin, P., Dorado, B., Freyss, M., Bertolus, M., Skorek, R., Noirot, J., Noirot, L., Kaitasov, O., Maillard, S., Apr. 2012. Nucleation and growth of intragranular defect and insoluble atom clusters in nuclear oxide fuels. NIMB 277 (0), 98. 2, 3, 5

[5] Govers, K., Bishop, C., Parfitt, D., Lemehov, S., Verwerft, M., Grimes, R., Jan. 2012. Molecular dynamics study of Xe bubble re-solution in UO2. Journal of Nuclear Materials 420 (1-3), 282–290. 9

[6] Huang, M., Schwen, D., Averback, R., Apr. 2010. Molecular dynamic simulation of fission fragment induced thermal spikes in UO2: Sputtering and bubble re-solution. Journal of Nuclear Materials 399 (2-3), 175–180. 9

[7] Kashibe, S., Une, K., Nogita, K., Nov. 1993. Formation and growth of intragranular fission gas bubbles in UO2 fuels with burnup of 6-83 GWd/t. JNM 206 (1), 22–34. 2

[8] Lanore, J.-M., Jan. 1974. Simulation de l'evolution des defauts dans un reseau par le methode de monte-carlo. Rad. Eff. 22 (3), 153–162. 5

[9] Maillard, S., Skorek, R., Maugis, P., Dumont, M., 2015. Rate theory. OCDE Report. 5

[10] Martin, G., Garcia, P., Sabathier, C., Van Brutzel, L., Dorado, B., Garrido, F., Maillard, S., Jul. 2010. Irradiation-induced heterogeneous nucleation in uranium dioxide. PLA 374 (30), 3038. 3, 4

[11] Martin, G., Garcia, P., Van Brutzel, L., Dorado, B., Maillard, S., Jul. 2011. Effect of the cascade energy on defect production in uranium dioxide. NIMB 269 (14), 1727. 3, 5

[12] Martin, G., Maillard, S., Brutzel, L. V., Garcia, P., Dorado, B., Valot, C., Mar. 2009. A molecular dynamics study of radiation induced diffusion in uranium dioxide. JNM 385 (2), 351. 3, 7

[13] Martin, G., Sabathier, Wiktor, Maillard, 2015. Molecular dynamics study of the bulk temperature effect on primary radiation damage in uranium dioxide. NIMB 352, 135. 5

[14] Matzke, H., Aug. 1983. Radiation enhanced diffusion in UO2 and (U, Pu)O2. Radiation Effects and Defects in Solids 75, 317–325. 7

[15] Michel, A., Sabathier, C., Carlot, G., Kaïtasov, O., Bouffard, S., Garcia, P., Valot, C., 2012. An in situ TEM study of the evolution of Xe bubble populations in UO2. NIMB 272, 218–221. 2

[16] Nelson, R. S., Jun. 1969. The stability of gas bubbles in an irradiation environment. Journal of Nuclear Materials 31 (2), 153–161. 9

[17] Noirot, L., 2006. MARGARET: An Advanced Mechanistic Model of Fission Gas Behavior in Nuclear Fuel. Journal of Nuclear Science and Technology 43 (9), 1149–1160. 9

[18] Olander, D., 1976. Fundamental Aspects of Nuclear Reactor Fuel Elements. 9

[19] Russell, K. C., Oct. 1978. The theory of void nucleation in metals. Acta Metallurgica 26 (10), 1615–1630. 8

[20] Sabathier, C., Michel, A., Carlot, G., Martin, G., Maillard, S., Bachelet, C., Fortuna, F., Kaitasov, O., Oliviero, E., Garcia, P., 2014. In-situ TEM observation of nano-void formation in UO2 under irradiation. NIMB 326, 247–250. 5, 6

[21] Sabathier, C., Vincent, L., Garcia, P., Garrido, F., Carlot, G., Thome, L., Martin, P., Valot, C., Jun. 2008. In situ TEM study of temperature-induced fission product precipitation in UO2. Nuclear Instruments and Methods in Physics Research Section B: Beam Interactions with Materials and Atoms 266 (12-13), 3027–3032. 2

[22] Schwen, D., Huang, M., Bellon, P., Averback, R., Jul. 2009. Molecular dynamics simulation of intragranular Xe bubble re-solution in UO2. JNM 392 (1), 35–39. 9

[23] Simeone, D., Luneville, L., Serruys, Y., Jul. 2010. Cascade fragmentation under ion beam irradiation: A fractal approach. Phys. Rev. E 82 (1), 011122. 3, 5

[24] Skorek, R., 2013. Étude par Dynamique d'Amas de l'influence des défauts d'irradiation sur la migration des gaz de fission dans le dioxyde d'uranium. PhD Thesis, Univ. Aix - Marseille. 5, 14

[25] Soullard, J., Oct. 1985. High voltage electron microscope observations of UO2. JNM 135 (2-3), 190–196. 5, 14

[26] Turnbull, J., Feb. 1971. The distribution of intragranular fission gas bubbles in UO_2 during irradiation. JNM 38 (2), 203–212. 2

[27] Van Brutzel, L., Rarivomanantsoa, M., Nov. 2006. Molecular dynamics simulation study of primary damage in UO2 produced by cascade overlaps. JNM 358 (2-3), 209–216. 3

[28] Van Brutzel, L., Rarivomanantsoa, M., Ghaleb, D., Aug. 2006. Displacement cascade initiated with the realistic energy of the recoil nucleus in UO2 matrix by molecular dynamics simulation. JNM 354 (1-3), 28–35. 3

[29] Vathonne, E., 2014. Étude par calcul de structure électronique des dégâts d'irradiation dans le combustible nucléaire UO2 : comportement des défauts ponctuels et gaz de fssion. Ph.D. thesis. 7

[30] Veshchunov, M. S., Jan. 2000. On the theory of fission gas bubble evolution in irradiated UO2 fuel. Journal of Nuclear Materials 277 (1), 67–81. 8

[31] Ziegler, Biersack, Littmark, 2012. SRIM: The stopping and range of ions in matter. 6

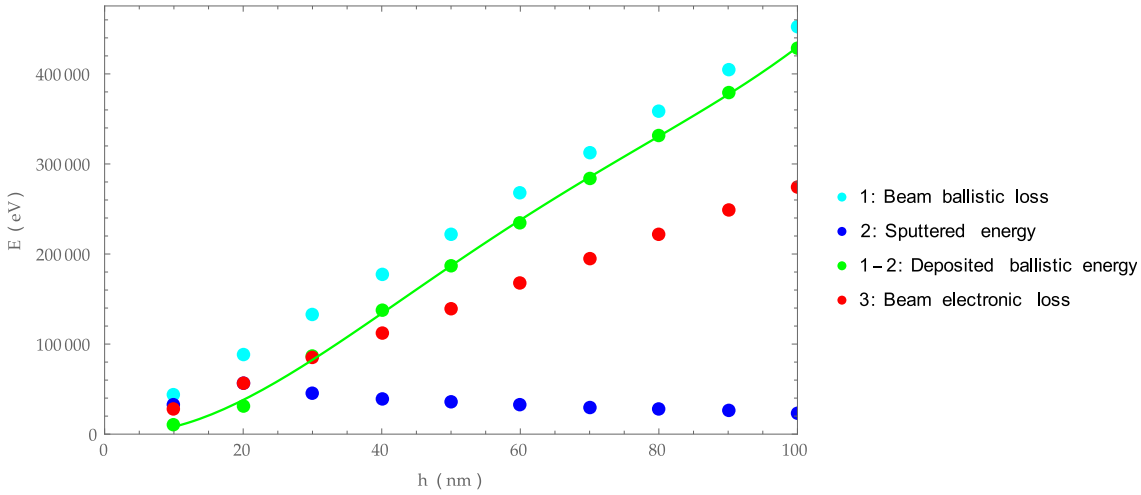

Figure 1: Deposited ballistic energy (difference between the beam ballistic loss and the sputtered energy) as a function of the foil thickness.

		Experiment parameters
h	20 nm	Foil thickness
E_b	31 keV	Ballistic energy transferred to the foil (taking account of the sputtering): $E_b\,(\text{eV}) = 3321.17 - 1146.41h + 184.607h^2 - 2.22491h^3 + 0.00919919h^4$, h (nm) (Fig 1)
E_s	25 keV	Sub-cascade energy
F		Fluency
Δt_b	0.06 s	Average time between 2 sub-cascades in the simulation cell
T	300 K	Temperature
		Sub-cascade model parameters
n^s	3375	Number of voxels for the disordered zone
n^c	3	Number of voxels for the clusters (cavity and loop) nucleated in the sub-cascade
n^p	47	Number of pairs (Schottky/anti-Schottky) of isolated defects (1 voxel) per sub-cascade
N^t	10^6	Number of voxels for the simulation cell
		UO_2 related physical properties
E^m	0.7 eV	Migration energy for anti-Schottky defect [24, 25]
D_0	1.22×10^{12} nm^2/s	Diffusivity coefficient at room temperature, $T = 300$ K ($D = D_0 e^{-\frac{E_m}{kT}}$) [24]
V	0.0427 nm^3	Volume of the Schottky defect
a	0.555 nm	Size ot the Schottky defect considered as a cube: $V = a^3$
V^s	150 nm^3	Volume of the disordered zone $V^s = n^s V$
V^c	0.176 nm^3	Volume of the cluster $V^c = n^c V$
V^t	43961 nm^3	Volume of the simulation cell $V^t = N^t V$

Table 1: Parameters for the simulation (implantation of 4 MeV Au atoms).

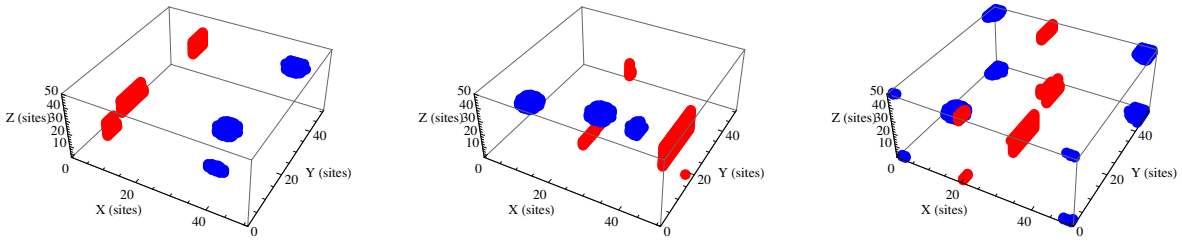

Figure 2: Example of micro-structure after 2, 5 and 10 sub-cascades, the isolated defects are omitted. For example , periodic boundary conditions can be seen in the first image where a loop and a cavity are split two ways.

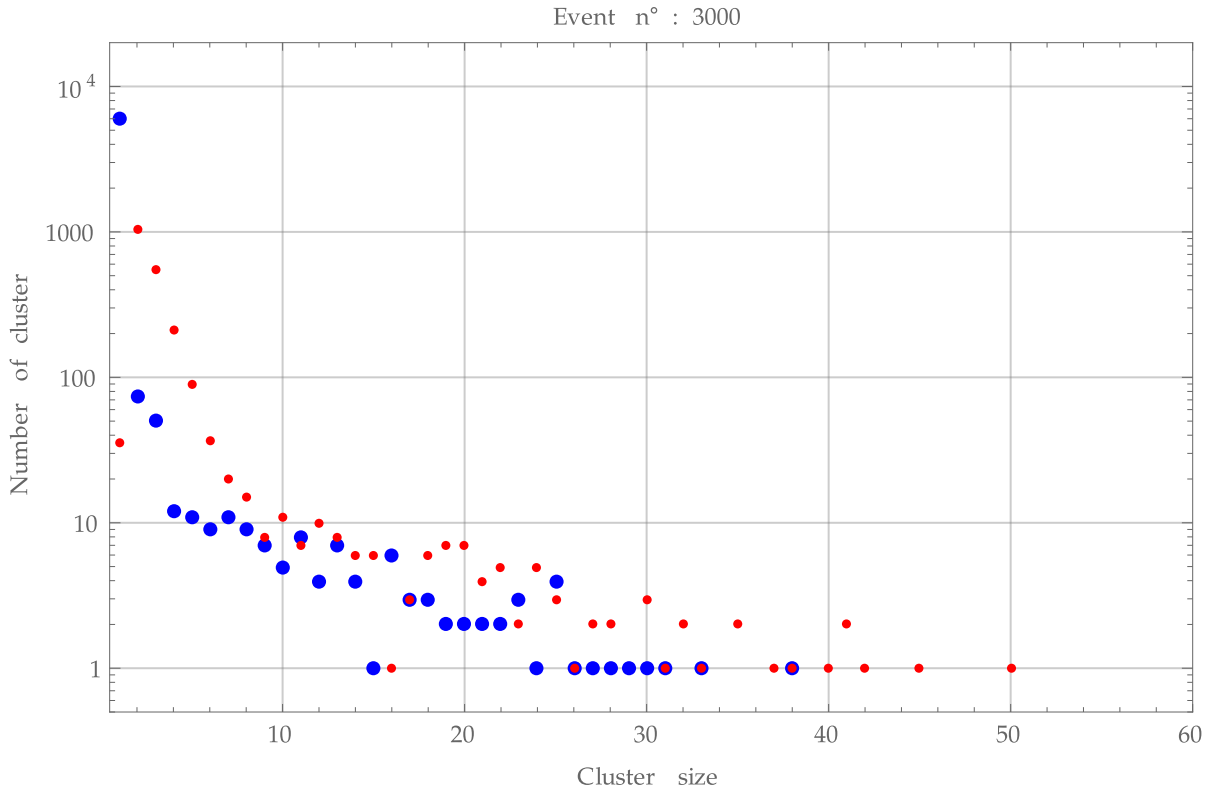

Figure 3: Cluster size distribution after 3000 iterations ($F \sim 1\,\mathrm{nm}^{-2}$). The blue and red dots correspond to cavities and loops.

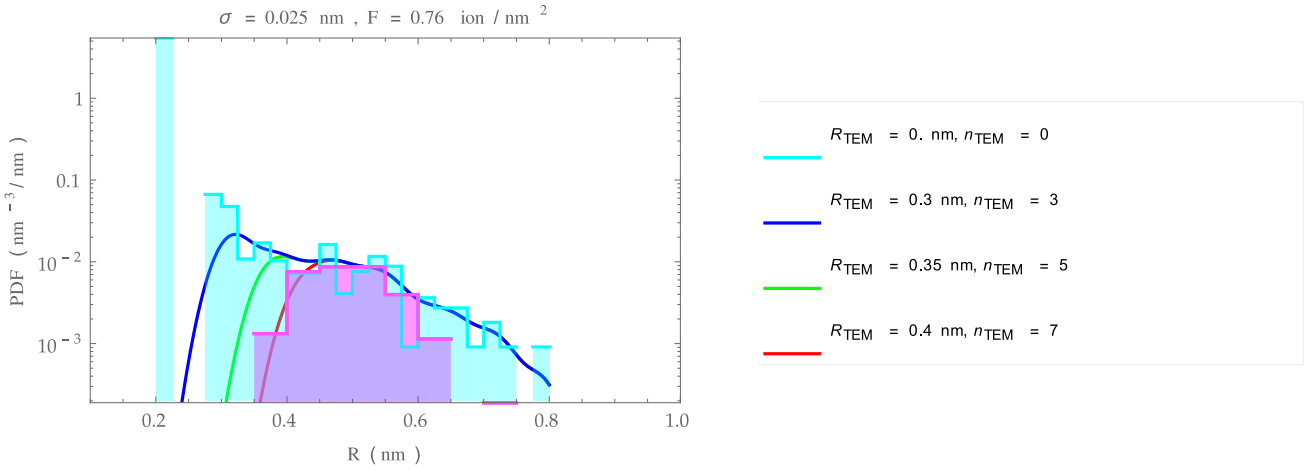

Figure 4: Impact of the TEM sensitivity on the measured size distribution. The purple curve is the measured distribution (TEM observations) at a fluency $F \sim 0.76\,\mathrm{nm}^{-2}$. The light blue curve is the as simulated histogram of the distribution. The other curves (blue, green, red) describe the simulated distribution with various thresholds R_{TEM} for the TEM resolution and smoothed with a rms of 0.025 nm (corresponding to the camera resolution for the cavity limit).

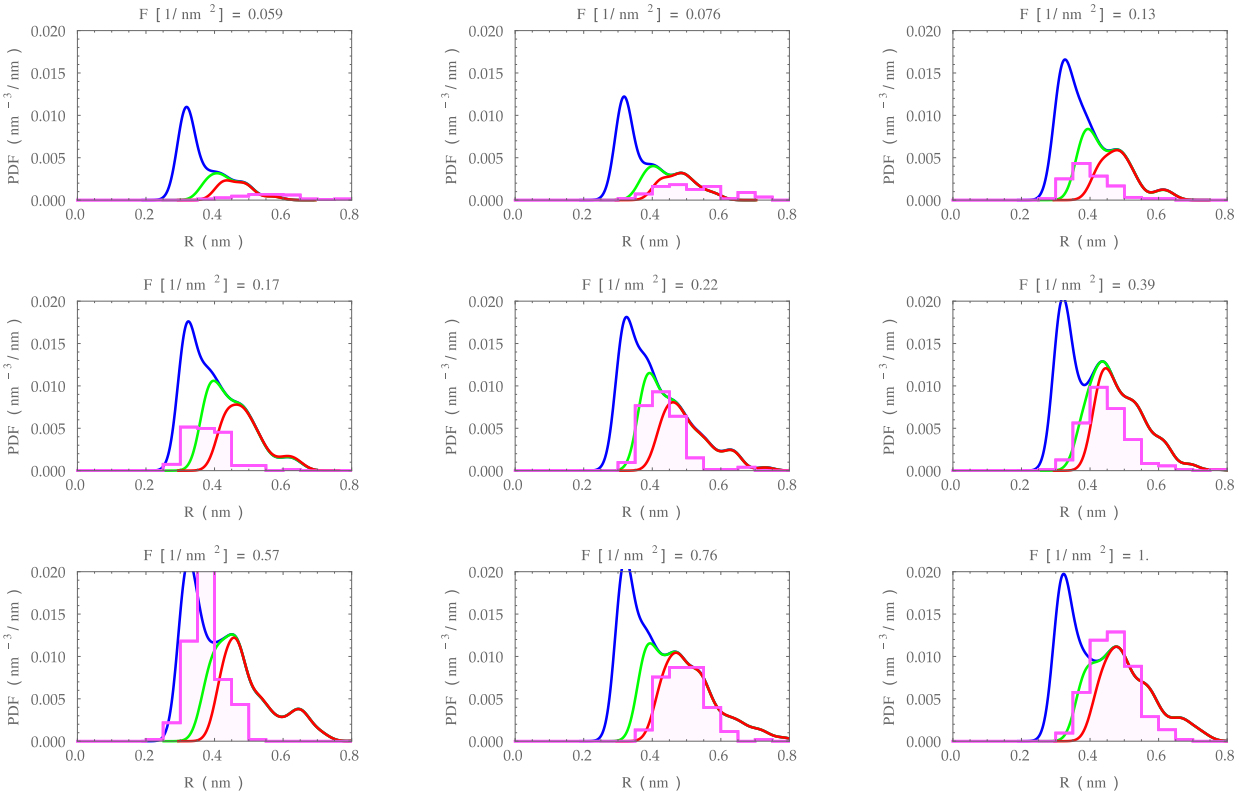

Figure 5: Snapshots at various fluencies of the simulated (with $R_{TEM} = 0.30$, 0.35, 0.40 nm) and measured size distributions (see Figure 4 for colors).

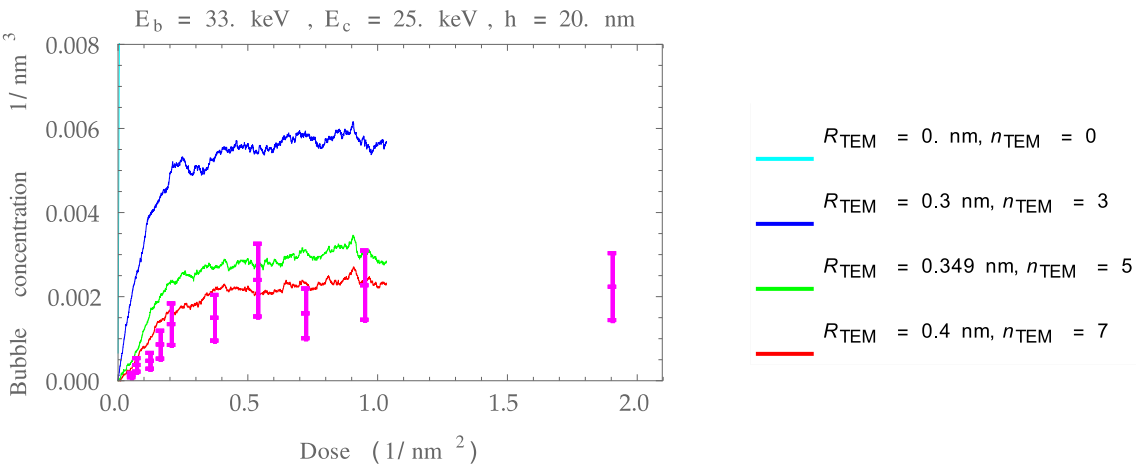

Figure 6: Evolution of the concentration of the cavities larger than some threshold values $R_{TEM} = 0.$, 0.30, 0.35, 0.40 nm.